Deterministic Role of Collision Cascade Density in Radiation Defect Dynamics in Si

J. B. Wallace,[1,2] L. B. Bayu Aji,[1] L. Shao,[2] and S. O. Kucheyev[1,*]
[1]Lawrence Livermore National Laboratory, Livermore, California 94550, USA
[2]Department of Nuclear Engineering, Texas A&M University, College Station, Texas 77843, USA

(Received 5 January 2018; published 25 May 2018)

The formation of stable radiation damage in solids often proceeds via complex dynamic annealing (DA) processes, involving point defect migration and interaction. The dependence of DA on irradiation conditions remains poorly understood even for Si. Here, we use a pulsed ion beam method to study defect interaction dynamics in Si bombarded in the temperature range from ~ -30 °C to 210 °C with ions in a wide range of masses, from Ne to Xe, creating collision cascades with different densities. We demonstrate that the complexity of the influence of irradiation conditions on defect dynamics can be reduced to a deterministic effect of a single parameter, the average cascade density, calculated by taking into account the fractal nature of collision cascades. For each ion species, the DA rate exhibits two well-defined Arrhenius regions where different DA mechanisms dominate. These two regions intersect at a critical temperature, which depends linearly on the cascade density. The low-temperature DA regime is characterized by an activation energy of ~0.1 eV, independent of the cascade density. The high-temperature regime, however, exhibits a change in the dominant DA process for cascade densities above ~0.04 at.%, evidenced by an increase in the activation energy. These results clearly demonstrate a crucial role of the collision cascade density and can be used to predict radiation defect dynamics in Si.

DOI: 10.1103/PhysRevLett.120.216101

The formation of stable radiation damage in solids often proceeds via so-called dynamic annealing (DA) processes, involving migration, recombination, and clustering of mobile point defects *during* irradiation [1–7]. The efficiency of DA depends nontrivially on irradiation conditions, including ion energy, mass, dose, dose rate, and target temperature (T). Because of such complexity, our understanding of DA remains limited even for Si, which is arguably the most extensively studied material [8].

Since the mobility of radiation-generated point defects is often thermally activated, DA processes can be quantified by measuring their activation energies (E_a's). However, previous investigations [1,3,9,10] of the effect of ion mass on DA in Si have revealed complex behavior with a wide spectrum of E_a's, ranging from ~0.2 to 1.7 eV, depending on ion mass, target T, and the measurement method used. For example, Goldberg *et al.* [3], building on the work of Schultz *et al.* [1], systematically studied the onset of bulk amorphization in Si bombarded with 80 keV ions with masses from ^{12}C to ^{132}Xe at T's from ~10 °C to 300 °C. They [3] found E_a's in a wide range of ~0.7–1.7 eV, increasing close to linearly with either ion mass or T. In another systematic study, Kinomura *et al.* [10], following the work of Linnros *et al.* [9], measured T dependencies of the rate of ion-beam-induced epitaxial crystallization and found E_a values of ~0.2–0.4 eV in the T range of ~150 °C–400 °C for irradiation with 3 MeV C, Si, Ge, or Au ions.

As discussed in detail recently [7], such inconsistency in E_a values can be understood by noting that, in all these previous studies [1,3,9,10], the dose rate was used as the rate of the kinetic process in the Arrhenius relationship. In this case, E_a's are effectively extracted from T dependencies of the DA efficiency (that reflects the fraction of ballistically generated Frenkel defects that participate in DA) rather than of the DA rate [7].

To circumvent this problem, DA rates in Si were recently studied by a pulsed ion beam method [5–7]. In this method, a continuous ion beam is split into a train of equal square pulses, and the time constant of DA is measured directly by studying lattice disorder as a function of the time interval between adjacent pulses, with all the other irradiation parameters kept constant. Measurements of T dependencies of the DA rate in Si bombarded with 500 keV Ar ions have revealed two well-defined regimes with E_a's of ~0.1 and ~0.4 eV, below and above a critical temperature (T_c) of ~60 °C, respectively [7]. These experimental results together with rate theory modeling have pointed to a crucial role of the migration of Frenkel pair defects in intercascade DA in Ar-ion bombarded Si [7]. However, many questions remain unanswered. In particular, are these two E_a's of 0.1 and 0.4 eV and a T_c of 60 °C relevant only for the case of Ar-ion bombardment or are they fundamental parameters that can be used to predict radiation defect dynamics in Si for a wide range of irradiation conditions with different collision cascade densities?

Here, we answer the above questions via a systematic study of T-dependent DA rates in Si bombarded with ions with masses from ^{20}Ne to ^{129}Xe. We analyze experimental

data with a recently developed model that captures the fractal nature of ballistic collision cascades [11]. Our results demonstrate that the complex dependencies of radiation defect dynamics on ion mass, energy, and depth from the sample surface can be reduced to a single dependence on the average cascade density (ρ) computed for any given set of irradiation conditions.

The 4 MV ion accelerator (National Electrostatics Corporation, model 4UH) at Lawrence Livermore National Laboratory was used for both ion irradiation and ion beam analysis. Float-zone grown (100) Si single crystals (with a resistivity of ~5 Ω cm) were bombarded with 500 keV $^{20}Ne^+$, $^{84}Kr^+$, or $^{129}Xe^+$ ions at 7° off the [100] direction in the T range from −30 °C to 210 °C. For completeness, we also analyze data for pulsed beam bombardment of Si with 500 keV $^{40}Ar^+$ ions reported previously [5,7]. To improve thermal contact, the samples were attached to a Cu sample holder with conductive Ag paste. All irradiations were performed in a broad beam mode (rather than with rastered beams) [5]. The total ion dose was split into a train of equal square pulses with instantaneous dose rates (F_{on}) of 2.7×10^{13}, 1.9×10^{13}, 0.8×10^{13}, and 0.45×10^{13} $cm^{-2}\,s^{-1}$ for Ne, Ar, Kr, and Xe, respectively. In each case, the pulse duration (t_{on}) was 1 ms. The adjacent pulses were separated by time t_{off}, which was varied between 0.1 and 100 ms. The inset in Fig. 1(b) shows a schematic of the time dependence of the instantaneous dose rate and defines pulsing parameters t_{on}, t_{off}, and F_{on}.

The dependence of lattice damage on t_{off} was studied *ex situ* at room T by ion channeling with 2 MeV $^4He^+$ ions incident along the [100] direction and backscattered into a detector at 164° relative to the incident beam direction. Raw channeling spectra were analyzed with one of the conventional algorithms [12] for extracting depth profiles of relative disorder. Values of average bulk relative disorder (n) were obtained by averaging depth profiles of relative disorder over 20 channels (~38 nm) centered on the bulk defect peak. Error bars of n are standard deviations. Total ion doses at different T's and ion masses were different and chosen such that, for continuous beam irradiation (i.e., $t_{off} = 0$), n was in the range of 0.6–0.9 (with $n = 1$ corresponding to full amorphization).

Three-dimensional distributions of ballistically generated lattice vacancies in Si were calculated with the TRIM code (version SRIM-2013.00, full cascade calculations) [13] with an atomic concentration of 5×10^{22} at cm^{-3} and a threshold energy for atomic displacement of 15 eV. For every ion species, ρ was calculated with a fractal model from Ref. [11] by averaging over ≳600 individual cascades. We defined ρ as the average local density of lattice vacancies within individual cascades with an averaging radius of 20 nm, which was chosen based on our recent estimates of the effective diffusion length of the mobile defects dominating DA in Si [11].

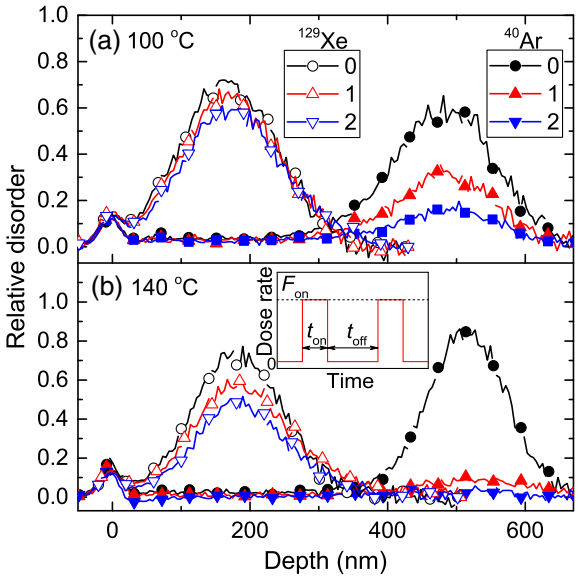

FIG. 1. Selected depth profiles of relative disorder in Si bombarded with pulsed beams of (closed symbols) 500 keV Ar and (open symbols) Xe ions with $F_{on} = 1.9 \times 10^{13}$ and 5.0×10^{12} $cm^{-2}\,s^{-1}$, respectively, $t_{on} = 1$ ms, and different t_{off} values given in legends (in units of 10^{-3} s) at temperatures of (a) 100 °C and (b) 140 °C. For clarity, only every 10th experimental point is depicted. The inset in (b) is a schematic of the time dependence of the instantaneous dose rate for pulsed beam irradiation, defining t_{on}, t_{off}, and F_{on}.

Figures 1(a) and 1(b) show representative depth profiles of relative disorder in Si bombarded at 100 °C and 140 °C, respectively, with continuous ($t_{off} = 0$ ms) or pulsed ($t_{off} = 1$ and 2 ms) beams of Ar or Xe ions. It is seen that, for both T's, these depth profiles are bimodal, with the first small peak at the sample surface, and the second major peak in the crystal bulk. The bulk defect peaks are centered on ~500 and 180 nm for Ar and Xe ions, respectively. These correspond to positions of the maxima of nuclear energy loss profiles (R_{pd}) for these ions [13]. Figure 1 further reveals that the average bulk disorder (n) decreases with increasing t_{off} at both T's and for both ion species. The decrease in n with increasing t_{off} is, however, much larger for the case of lighter Ar than for heavier Xe ion irradiation, reflecting a decrease in the DA efficiency with increasing ion mass. All these observations are in qualitative agreement with results of our previous pulsed beam study of Si at room T [6].

Figure 2 summarizes $n(t_{off})$ dependencies for T's in the range from −30 °C to 210 °C for Xe, Kr, and Ne ions. It is seen that, for all the T's and ion species studied, n monotonically decreases with increasing t_{off}. This effect is due to intercascade DA that involves the interaction of mobile defects generated in different pulses and, hence, in different collision cascades. Solid lines in Fig. 2 are fits of the data via the Marquardt-Levenberg algorithm [14] with the first order decay equation, $n(t_{off}) = n_\infty + [n(0) - n_\infty]\exp(-t_{off}/\tau)$, with τ and n_∞ as the fitting parameters. Here, τ is the DA

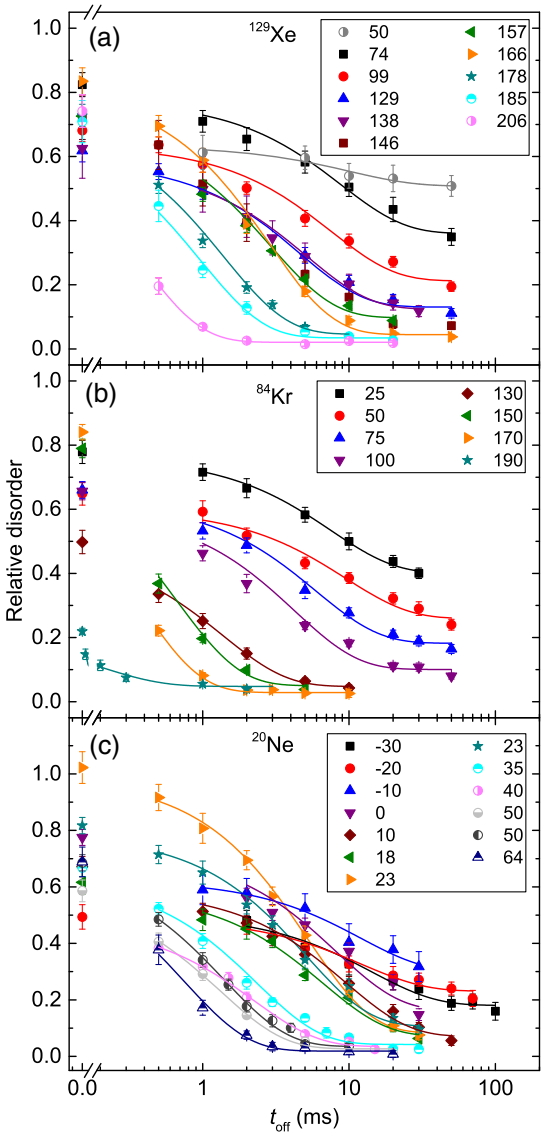

FIG. 2. Average relative bulk disorder in Si bombarded at different temperatures (given in legends in units of °C) with pulsed beams of 500 keV (a) Xe, (b) Kr, and (c) Ne ions with F_{on} of 0.45×10^{13}, 0.8×10^{13}, and 2.7×10^{13} cm^{-2} s^{-1}, respectively, and $t_{on} = 1$ ms as a function of the passive portion of the beam duty cycle (t_{off}). Solid lines show results of fitting with the first order decay equation.

time constant, and n_∞ is relative bulk disorder for $t_{off} \gg \tau$. In all the cases, R-squared values of the fitting were > 0.96.

In Fig. 3, we plot $\tau(T)$ dependencies, obtained by fitting $n(t_{off})$ data from Fig. 2 (and from Ref. [7] for Ar ions), in the Arrhenius coordinates, with the DA rate defined as τ^{-1} for a first order decay process, and with kT having the usual meaning. It reveals a monotonic decrease of τ with increasing T or decreasing ion mass (and, hence, ρ). Figure 3 provides evidence that DA processes are thermally activated in the entire range of ion masses studied, in qualitative agreement with previous studies of DA in Si [1,3,7,9,10].

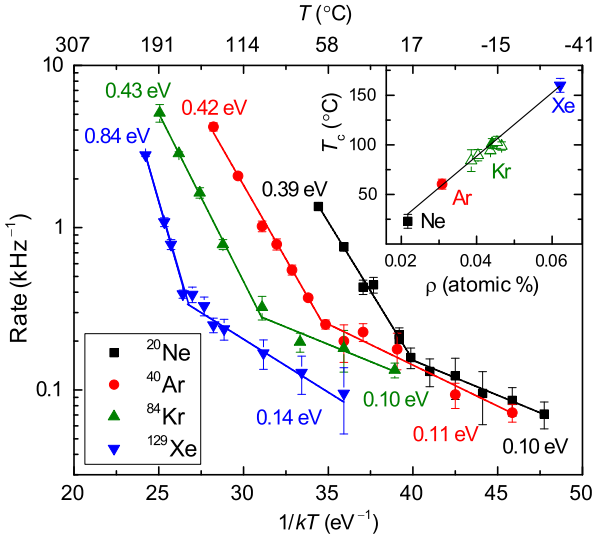

FIG. 3. Arrhenius plot of the DA rate for Si bombarded with pulsed beams of Ne, Ar, Kr, and Xe ions. Straight lines show results of linear fitting, revealing the low- and high-T activation energies shown. The inset shows the critical temperature (T_c), separating the two DA regimes, as a function of the average cascade density (ρ) at depths corresponding to R_{pd}'s. Open symbols for Kr ions are T_c values at different depths between ~150 and 400 nm.

Figure 3 further reveals that, for each ion mass, two Arrhenius regimes are clearly seen with very different E_a's, defined by slopes obtained by fitting the data with the Arrhenius equation: $\tau^{-1} = A \exp(-E_a/kT)$, where A is the preexponential factor. We will refer to these two Arrhenius regimes as high- and low-T regimes. Fitting the data gives the high-T A's of 5.2×10^{12}, 8.0×10^{8}, 5.2×10^{8}, and 1.0×10^{9} Hz and the low-T A's of 3.5×10^{4}, 5.1×10^{3}, 1.5×10^{4}, and 7.9×10^{3} Hz for Ne, Ar, Kr, and Xe ions, respectively. The low-T E_a is ~0.1 eV for all the ion species studied, while the high-T E_a is ~0.4 eV for Ne, Ar, and Kr, and it doubles for the case of Xe. Figure 3 also shows that, for each ion mass, the two Arrhenius regimes are separated by T_c, which increases with increasing ion mass and, hence, the cascade density (ρ). This effect is better illustrated in the inset in Fig. 3, revealing a linear $T_c(\rho)$ dependence.

Rate theory modeling in our previous study of Si bombarded with 500 keV Ar ions [7] has attributed the high-T E_a of 0.4 eV to the rate-limiting migration of vacancies, which is consistent with a number of previous studies of vacancy diffusion in Si [15–17]. The low-T E_a of 0.1 eV has been associated with the rate-limiting formation of divacancies as the main channel of vacancy annihilation [7]. The fact that DA for bombardment with different ion species, generating cascades in a wide range of ρ's, is characterized by the same low-T E_a of 0.1 eV (Fig. 3) strongly suggests that the rate-limiting DA processes are ρ independent in this T regime.

In contrast, Fig. 3 shows that, for the high-T regime, E_a doubles on increasing ion mass from Kr to Xe. First, we note that such a difference in the high-T E_a for Xe and the other ions cannot be attributed simply to a change in T, as in previous experiments of Goldberg *et al.* [3]. Indeed, the T ranges for Kr and Xe bombardment in Fig. 3 overlap significantly. Such a large change in E_a on increasing ion mass from Kr to Xe can be understood by examining depth-dependencies of τ, T_c, and ρ. Indeed, ρ is strongly depth dependent. Closer to the sample surface, away from the R_{pd}, ion energy is higher, and the cross section for elastic collisions is lower, leading to lower ρ. This is illustrated by Fig. 4 (left axis, closed symbols), which compares depth profiles of ρ for Kr and Xe ions. It shows that the shape of such profiles is similar to that of nuclear energy loss distributions. The maximum ρ occurs at ~300 and 180 nm for Kr and Xe ions, respectively, and ρ rapidly decreases toward the surface. The vertical dashed line at ~45 nm in Fig. 4 shows the depth at which ρ for Xe is equal to the maximum ρ for Kr. If the change in the high-T E_a observed for Xe ions is a ρ-related effect, E_a is expected to decrease to ~0.4 eV at depths $\lesssim$45 nm.

Figure 4 (right axis, open symbols) tests this hypothesis and shows depth dependencies of the high-T E_a for Kr and Xe ions. The E_a for Kr is approximately constant in the entire depth range studied (~100–400 nm), while, in the same depth range, T_c for the same Kr ions decreases with decreasing ρ toward the surface, as shown by open symbols in the inset of Fig. 3. The T_c data points obtained by the analysis of Kr-ion-induced damage at depths away from the R_{pd} fall onto the same linear $T_c(\rho)$ dependence defined by points measured at R_{pd}'s for cases of bombardment with different ion masses. This further supports that ρ is the fundamental parameter determining T_c. Our analysis of depth-dependent data has also shown that the low-T E_a of 0.1 eV for both Xe and Kr is, within error bars, independent of depth.

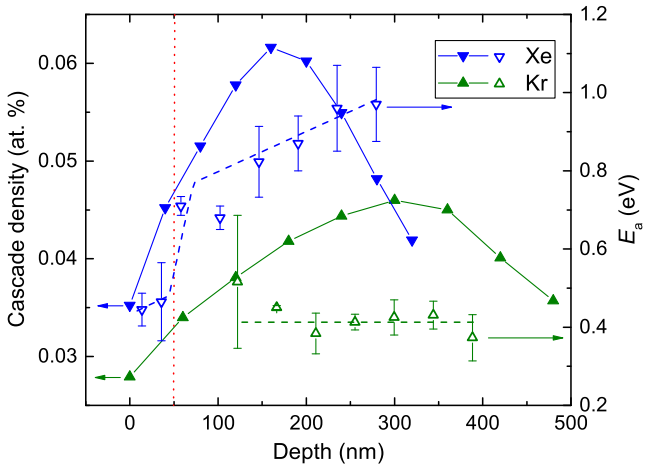

FIG. 4. Depth dependencies of (left axis, closed symbols) the average cascade density and (right axis, open symbols) the high-T E_a in Si bombarded with 500 keV Kr or Xe ions, as indicated in the legend. The vertical dashed line denotes the depth at which the cascade density for Xe ions equals the peak cascade density for Kr ions. Dashed lines through E_a dependencies are to guide the eye.

In contrast to the case of Kr, Fig. 4 (right axis) shows that the high-T E_a for Xe ions decreases close to linearly from ~0.95 eV at ~300 nm (which is well beyond the maximum of the bulk relative disorder at $R_{pd} = 180$ nm) to ~0.7 eV at ~100 nm. At shallower depths, where $\rho \lesssim 0.045$ at.%, the high-T E_a for Xe reduces more rapidly to ~0.45 eV. Hence, for cascades with $\rho \lesssim 0.045$ at.%, DA appears to be rate limited by the migration of Frenkel pair defects as discussed above [7]. For denser cascades, a different high-T DA mechanism characterized by a larger and ρ-dependent E_a becomes dominant. This high-cascade-density regime could be associated with the onset of collective phenomena of the formation of energy spikes (i.e., thermal and/or displacement spikes) [18]. Such energy spikes lead to the formation of zones of heavily disordered or amorphous material. The new thermally activated DA mechanism with a high E_a could involve processes of defect interaction with the defective zones formed in energy spikes. Specific DA mechanisms in the regime of dense collision cascades could be revealed in future theoretical and modeling work benchmarked against our experimental data. These ρ-driven defect interaction dynamics phenomena also call for future systematic high-depth resolution and high-precision measurements with an extended range of ρ values produced by heavier and/or cluster ions.

This work was funded by the Nuclear Energy Enabling Technology (NEET) Program of the U.S. DOE, Office of Nuclear Energy and performed under the auspices of the U.S. DOE by LLNL under Contract No. DE-AC52-07NA27344. J. B. W would like to acknowledge the LGSP for funding.

*kucheyev@llnl.gov

[1] P. J. Schultz, C. Jagadish, M. C. Ridgway, R. G. Elliman, and J. S. Williams, Phys. Rev. B **44**, 9118 (1991).
[2] B. G. Svensson, C. Jagadish, and J. S. Williams, Phys. Rev. Lett. **71**, 1860 (1993).
[3] R. D. Goldberg, J. S. Williams, and R. G. Elliman, Nucl. Instrum. Methods Phys. Res., Sect. B **106**, 242 (1995).
[4] R. D. Goldberg, J. S. Williams, and R. G. Elliman, Phys. Rev. Lett. **82**, 771 (1999).
[5] M. T. Myers, S. Charnvanichborikarn, L. Shao, and S. O. Kucheyev, Phys. Rev. Lett. **109**, 095502 (2012).
[6] J. B. Wallace, L. B. Bayu Aji, L. Shao, and S. O. Kucheyev, J. Appl. Phys. **118**, 135709 (2015).
[7] J. B. Wallace, L. B. Bayu Aji, A. A. Martin, S. J. Shin, L. Shao, and S. O. Kucheyev, Sci. Rep. **7**, 39754 (2017).
[8] L. Pelaz, L. A. Marques, and J. Barbolla, J. Appl. Phys. **96**, 5947 (2004).

[9] J. Linnros, B. Svensson, and G. Holmen, Phys. Rev. B **30**, 3629 (1984).
[10] A. Kinomura, J. S. Williams, and K. Fujii, Phys. Rev. B **59**, 15214 (1999).
[11] J. B. Wallace, L. B. Bayu Aji, L. Shao, and S. O. Kucheyev, Sci. Rep. **7**, 17574 (2017).
[12] K. Schmid, Radiat. Eff. **17**, 201 (1973).
[13] J. F. Ziegler, M. D. Ziegler, and J. P. Biersack, Nucl. Instrum. Methods Phys. Res., Sect. B **268**, 1818 (2010).
[14] K. Levenberg, Q. Appl. Math. **2**, 164 (1944).
[15] G. D. Watkins, Mater. Sci. Semicond. Process. **3**, 227 (2000).
[16] P. G. Coleman and C. P. Burrows, Phys. Rev. Lett. **98**, 265502 (2007).
[17] Y. Shimizu, M. Uematsu, and K. M. Itoh, Phys. Rev. Lett. **98**, 095901 (2007).
[18] D. A. Thompson, Radiat. Eff. **56**, 105 (1981).